Non-Monotonic Effect of Substrate Inhibition in Conjunction with Diffusion Limitation on the Response of Amperometric Biosensors

Romas Baronas *

Posted Date: 21 May 2025

doi: 10.20944/preprints202505.1693.v1

Keywords: amperometric biosensor; substrate inhibition; diffusion limitation; transient response; mathematical modeling; computational simulation

 doi:10.20944/preprints202505.1693.v1

Article

Non-Monotonic Effect of Substrate Inhibition in Conjunction with Diffusion Limitation on the Response of Amperometric Biosensors

Romas Baronas

Vilnius University, Faculty of Mathematics and Informatics, Institute of Computer Science, Didlaukio 47, LT-08303 Vilnius, Lithuania; romas.baronas@mif.vu.lt

Abstract: The non-monotonic behavior of amperometric enzyme-based biosensors under uncompetitive substrate inhibition is investigated computationally using a two-compartment model consisting of an enzyme layer and an outer diffusion layer. The model is based on a system of reaction-diffusion equations that includes a nonlinear term associated with non-Michaelis-Menten kinetics of the enzymatic reaction and accounts for the partitioning between layers. In addition to the known effect of substrate inhibition, where the maximum biosensor current differs from the steady-state output, it has been determined that external diffusion limitations can also cause the appearance of a local minimum in the current. At substrate concentrations greater than both the Michaelis-Menten constant and the inhibition constant, and in the presence of external diffusion limitation, the transient response of the biosensor, after immersion in the substrate solution, may follow a five-phase pattern depending on the model parameter values: it starts from zero, reaches a global or local maximum, decreases to a local minimum, increases again, and finally decreases to a steady intermediate value. The biosensor performance is analyzed numerically using the finite difference method.

Keywords: amperometric biosensor; substrate inhibition; diffusion limitation; transient response; mathematical modeling; computational simulation

1. Introduction

Enzyme-based amperometric biosensors were the first type of biosensors developed and remain the most popular due to their simplicity, ease of production, and low cost [1–3]. They measure changes in the output current at the working electrode caused by the direct oxidation or reduction of biochemical reaction products. The amperometric response is typically proportional to the analyte (substrate) concentration in a buffer solution [2,4–6]. These devices have found widespread applications in clinical, environmental, industrial, toxin detection and other fields [3,7–11].

Most biosensors operate according to the Michaelis-Menten kinetics scheme,

$$\mathrm{E} + \mathrm{S} \underset{k_{-1}}{\overset{k_1}{\rightleftharpoons}} \mathrm{ES} \xrightarrow{k_2} \mathrm{E} + \mathrm{P}, \tag{1}$$

where E is an enzyme, S is a substrate, ES is an enzyme-substrate complex, P is a reaction product, and k_1, k_{-1} and k_2 are the rate constants [2,4,5,7].

Often, the kinetics of the enzyme-based biosensors are much more complicated than in the simplest scheme (1). Different substances may act as inhibitors and cause a reduction in the rate of an enzyme-catalyzed reaction [6,8,12]. The substrate in many enzyme-catalyzed reactions behaves as an inhibitor. In addition to the scheme (1), the interaction of the enzyme-substrate complex (ES) with

 doi:10.20944/preprints202505.1693.v1

other substrate molecule (S) following the generation of a non-active inhibitory complex (ESI) may produce one of the simplest non-Michaelis-Menten scheme of the enzyme action,

$$\mathrm{ES} + \mathrm{S} \underset{k_{-3}}{\overset{k_3}{\rightleftharpoons}} \mathrm{ESI}, \tag{2}$$

k_3 and k_{-3} are the rate constants [2,3,6,8].

Understanding the kinetic peculiarities of biosensors is crucial in their design and optimization [13–15]. Mathematical modeling has proven to be a useful tool to study the effect of enzyme inhibition [10,11,16–20]. Various approaches have been applied for the biosensor modeling [21–25]. Actual biosensors with uncompetitive substrate inhibition have already been modeled at various, often steady-state, conditions [26–29]. The amperometric biosensors utilizing the enzyme with the substrate inhibition have also been modeled at the external diffusion limitation and the steady-state [10,16] as well as the transition conditions [25,30,31].

In particular, Kulys showed that a multi-steady-state response can be generated at the electrode surface under external diffusion limitations when the substrate concentration is much greater than the Michaelis-Menten constant, assuming an extremely thin enzyme layer [16]. However, to the best of our knowledge, only non-monotonic transient responses featuring a maximum followed by a final steady-state current have been simulated [19,26,30–33]. In such cases, the response typically follows a three-phase pattern: starting from zero, reaching a maximum, and finally decreasing to a steady value.

When modeling practical biosensors, multi-layer models are usually required to achieve sufficient accuracy of the model [26,34,35]. Nevertheless, even mono-layer models that neglect external mass transport by diffusion have still been used in various applications in recent years due to the model simplicity [18,19,33,36–40]. However, external mass transport by diffusion significantly influences the dynamics of the catalytic processes in enzyme-loaded systems in general and biosensor response and sensitivity in particular [9,41–45]. Fortunately, mass transport through several outer diffusion layers can be rather effectively approximated by a single diffusion layer with effective diffusion coefficients [46–48]. As a result, two-compartment models have been widely used in biosensor modeling [10,34,49–54].

The aim of this work was to investigate in detail the influence of substrate inhibition, in conjunction with internal and external diffusion limitations, on the transient response of enzyme-based amperometric biosensors. This study focuses on the conditions under which the transient response of the biosensor, after being immersed in a substrate solution, exhibits a complex, multi-phase pattern, characterized by the appearance of a local minimum, a local maximum, or even both.

At transient conditions, a biosensor is mathematically modeled by a two-compartment model comprising a mono-enzyme layer where the enzyme reaction as well as the mass transport by diffusion take place, and a diffusion-limiting region, where only the mass transport by diffusion takes place. The model is based on a system of reaction-diffusion equations that includes a nonlinear term associated with non-Michaelis-Menten kinetics of the enzymatic reaction and involves partitioning between layers. The performance of the treated system is analyzed numerically using the finite difference technique [55,56], and the simulation results are compared with previous studies on biosensors under substrate inhibition [16,19,26,30,31].

2. Mathematical and Computational Modelling

2.1. Biosensor Principal Structure

An amperometric biosensor is considered an electrode and a relatively thin layer of an enzyme (enzyme membrane) applied onto the electrode surface [2,4,6,7,9]. The model involves three regions: the enzyme layer, where the enzymatic reaction as well as the mass transport by diffusion takes place, a diffusion-limiting region where only the mass transport by diffusion takes place, and a convective region where the analyte concentration is maintained constant [30,31]. The schematic view of the

 doi:10.20944/preprints202505.1693.v1

modeled biosensor is presented in Figure 1, where d_1 and d_2 stand for the thicknesses of the enzyme and outer diffusion layers, respectively.

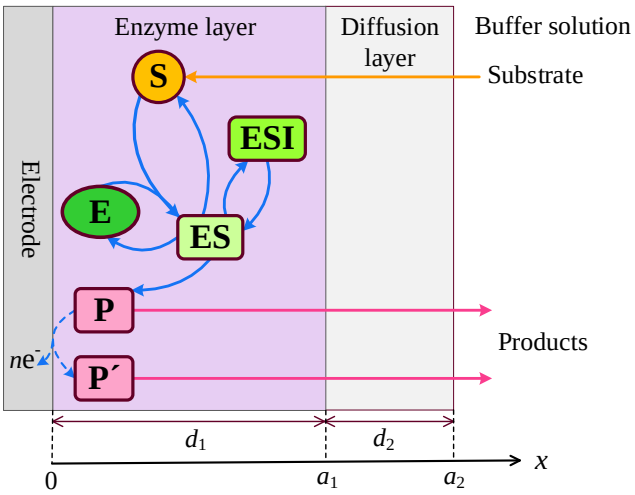

Figure 1. Schematic representation of the amperometric biosensor. The figure is not to scale.

In the enzyme layer, we consider the enzyme-catalyzed reactions (1) and (2). At the electrode surface, the electro-active product P is converted into a species P′ having no influence on the biosensor response, and electrons are released,

$$\mathrm{P} \rightarrow \mathrm{P}' \pm n\mathrm{e}^- \tag{3}$$

where n is the number of electrons transferred in the reaction.

Some reactions in the network (1), (2) and (3) are very fast, while others are considerably slower [2,4,6,7,9]. The large difference in timescales in the reaction network creates difficulties in simulating the temporal evolution of the network and for understanding the basic principles of its operation. To sidestep these problems, the quasi-steady-state approximation (QSSA) is often applied [57,58].

Assuming the QSSA, the concentration of the enzyme (E) and intermediate complexes (ES and ESI) do not change with time, and the rate of biochemical reaction is then expressed by the following equation of non-Michaelis-Menten kinetics:

$$\begin{aligned} V(S) &= \frac{V_{\max} S}{K_M + S + S^2/K_I}, \\ V_{\max} &= k_2 E_0, \quad K_M = (k_{-1} + k_2)/k_1, \quad K_I = k_{-3}/k_3, \end{aligned} \tag{4}$$

where S is the substrate concentration, $V_{\max}$ is the maximal enzymatic rate, E_0 is the total enzyme concentration, K_M is the Michaelis constant, and K_I is the inhibition constant (ESI dissociation constant) [4,31,59].

At so low substrate concentrations as $S \ll K_M$ and $S \ll K_I$, the nonlinear reaction rate in (4) reduces to the first-order reaction rate $V_{\max} S/K_M$, while at so high concentrations as $S \gg K_M$ and $S \ll K_I$, the rate becomes independent of the substrate concentration, i.e., zero-order kinetics. When $S > K_I$, the inhibitory term S^2/K_I in the denominator of the rate equation becomes significant, and the reaction rate starts to decline, even though substrate concentration is still increasing. The influence of inhibition on the overall biochemical process decreases with an increasing inhibition constant K_I, and the non-Michaelis-Menten kinetics approaches the Michaelis-Menten kinetics as $K_I \rightarrow \infty$. Focusing on the influence of substrate inhibition, the analysis is limited to substrate concentrations greater than the inhibition constant K_I.

In the two-compartment (two-layer) model, the diffusion layer is often treated as the Nernst diffusion layer [9,55,60]. But it can also be treated as a semi-permeable (diffusion-limiting) membrane

 doi:10.20944/preprints202505.1693.v1

if the outer Nernst diffusion is neglected [25,34,43,55,61], although the Nernst layer's zero thickness cannot be achieved in practice [62].

Sometimes, mathematical models of biosensors involve both the outer membrane and the Nernst diffusion layer [26,47,48,63]. However, the mass transport through several diffusion layers can be rather efficiently approximated by a single diffusion layer with effective diffusion coefficients, and a multi-compartment model can be reduced to a two-compartment model [46–48]. Therefore, the effects investigated here can also be applied to amperometric biosensors modeled by several diffusion layers including outer membranes and the Nernst diffusion layer.

2.2. Mathematical Model

Assuming symmetrical geometry of the electrode, enzymatic, and diffusion layers, along with a homogeneous distribution of the immobilized enzyme within the enzyme membrane, results in a two-compartment mathematical model defined in a one-dimensional spatial domain. This model is formulated as an initial boundary value problem that describes the dynamics of substrate and product concentrations [8,25,25,34,64].

2.2.1. Governing Equations

The dynamics of the concentrations of the substrate S and product P in the enzyme layer is described by a system of reaction-diffusion equations ($t > 0$),

$$\begin{aligned} \frac{\partial S_1}{\partial t} &= D_{S_1} \frac{\partial^2 S_1}{\partial x^2} - V(S_1), \\ \frac{\partial P_1}{\partial t} &= D_{P_1} \frac{\partial^2 P_1}{\partial x^2} + V(S_1), \quad x \in (0, a_1), \end{aligned} \tag{5}$$

where $S_1(x,t)$ and $P_1(x,t)$ are the concentrations of the substrate and the product in the enzyme layer, D_{S_1} and D_{P_1} are the diffusion coefficients, $d_1 = a_1$ is the thickness of the enzyme layer, and $V(S_1)$ is the reaction rate as defined in (4) [8,34,59].

Only the mass transport by diffusion of both compounds takes place in the diffusion layer ($t > 0$),

$$\begin{aligned} \frac{\partial S_2}{\partial t} &= D_{S_2} \frac{\partial^2 S_2}{\partial x^2}, \\ \frac{\partial P_2}{\partial t} &= D_{P_2} \frac{\partial^2 P_2}{\partial x^2}, \quad x \in (a_1, a_2), \end{aligned} \tag{6}$$

where $S_2(x,t)$ and $P_2(x,t)$ are the concentrations of the substrate and the reaction product, D_{S_2}, D_{P_2} are the diffusion coefficients, $a_2 = a_1 + d_2$, and d_2 is the thickness of the diffusion layer [8,25,34].

2.2.2. Boundary Conditions

In the bulk, the concentrations of the substrate and the product remain constant during the biosensor operation ($t > 0$),

$$S_2(a_2, t) = S_0, \quad P_2(a_2, t) = 0, \tag{7}$$

where S_0 is the concentration of the substrate in the bulk.

At the interface between adjacent layers, the exiting and entering fluxes of the substrate and product are assumed to be equal, while the concentrations on either side of the interface are related through formal partition coefficients θ_S and θ_P ($t > 0$ [63–67],

$$\begin{aligned} D_{S_1} \frac{\partial S_1}{\partial x}\Big|_{x=a_1} &= D_{S_2} \frac{\partial S_2}{\partial x}\Big|_{x=a_1}, \quad S_1(a_1,t) = \theta_S S_2(a_1,t), \\ D_{P_1} \frac{\partial P_1}{\partial x}\Big|_{x=a_1} &= D_{P_2} \frac{\partial P_1}{\partial x}\Big|_{x=a_1}, \quad P_1(a_1,t) = \theta_P P_2(a_1,t). \end{aligned} \tag{8}$$

 doi:10.20944/preprints202505.1693.v1

The partition coefficients are generally different for different species [66,68], but they are often assumed to be identical [10,48,53,63,65].

Due to the electrochemical reaction (3), the concentration of the reaction product drops down at the electrode surface, while the substrate is assumed to be electrically inactive, and no concentration flux is considered for it ($t > 0$) [8,34,69],

$$P_1(0,t) = 0, \quad D_{S_1} \frac{\partial S_1}{\partial x}\Big|_{x=0} = 0, \quad t > 0. \tag{9}$$

2.2.3. Initial Conditions

Two different initial conditions corresponding to two modes of biosensor operation are considered.

In the first mode, the biosensor is assumed to be permanently immersed in a buffer solution, and its operation begins when the analyte (substrate) is introduced at $t = 0$ into the buffer solution,

$$\begin{aligned} &S_1(x,0) = 0, \quad P_1(x,0) = 0, \quad x \in [0, a_1], \\ &S_2(x,0) = 0, \quad P_2(x,0) = 0, \quad x \in [a_1, a_2), \\ &S_2(a_2, 0) = S_0, \quad P_2(a_2, 0) = 0. \end{aligned} \tag{10}$$

This setup simulates injection analysis (IA) or real-time monitoring, where the analyte arrival initiates the biosensor transient response [8–10,18,26,51,70].

The second type of operation is common in batch analysis (BA) when the biosensor is directly immersed in a buffer solution containing the analyte [8,9,20,53,71]. The biosensor operation starts responding to the analyte from the moment of immersion. In this case, initial conditions (10) have to be replaced with

$$\begin{aligned} &S_1(x,0) = 0, \quad P_1(x,0) = 0, \quad x \in [0, a_1), \\ &S_1(a_1, 0) = \theta_S S_0, \quad P_1(a_1, 0) = 0, \\ &S_2(x,0) = S_0, \quad P_2(x,0) = 0, \quad x \in [a_1, a_2]. \end{aligned} \tag{11}$$

Let us notice that both initial conditions, (10) and (11), result in the same steady-state solution for the problem (5)–(9). Only the transient solution is affected by the initial conditions [8,25,34,55].

The two-compartment model (5)–(11) approaches the corresponding one-compartment model when $a_2 \to a_1$ ($d_2 \to 0$) [18,33,36,37,39,40].

2.3. Biosensor Response

The amperometric electrode measures the faradaic anodic or cathodic current [2,8,59]. The density $I(t)$ of the output current at time t can be obtained explicitly from Faraday's and Fick's laws,

$$I(t) = nFD_{P_1} \frac{\partial P_1}{\partial x}\Big|_{x=0}, \tag{12}$$

where n is the number of electrons involved in a charge transfer at the electrode surface, and F is the Faraday constant [8,34,69].

The system (5)-(9) approaches a steady-state as $t \to \infty$ [8,34,59],

$$I_{ss} = \lim_{t\to\infty} I(t), \tag{13}$$

where I_{ss} is the density of the steady-state output current.

Since the transient current in the case of the enzyme inhibition can be a non-monotonic function of time, the maximal current has also been used as a characteristic for this kind of biosensor [19,26,30–33]. Aiming to determine conditions under which biosensor response follows a multi-phase pattern, the number N_{ext} of extrema in transient output current $I(t)$ was studied. A local or global maximum of

 doi:10.20944/preprints202505.1693.v1

otput current $I(t)$ occurs at time $t = t_e$ if $I(t_e) \geq I(t)$ for all t near t_e, while a local minimum occurs at that time $t = t_e$ if $I(t_e) \leq I(t)$ for all t near t_e. N_{ext} is considered as the total count of maxima and minima that the function $I(t)$ has at $t > 0$,

$$N_{\text{ext}} = \left| \left\{ t > 0 \;\middle|\; \frac{\mathrm{d}I(t)}{\mathrm{d}t} = 0 \text{ and } \frac{\mathrm{d}^2 I(t)}{\mathrm{d}t^2} \neq 0 \right\} \right|, \tag{14}$$

where $|\cdot|$ denotes the set cardinality and the condition for defining the set.

In the specific case of a monotonic output current $I(t)$, $N_{\text{ext}} = 0$. In the case of a three-phase pattern, when the output current starts from zero, reaches a maximum, and then decreases to a steady value, $N_{\text{ext}} = 1$. $N_{\text{ext}} = 2$ when the biosensor response approaches a four-phase pattern, exhibiting a local minimum in addition to the maximum.

2.4. Dimensionless Model Parameters

In order to obtain the main governing parameters of the mathematical model, a dimensionless model is typically derived [60,63]. The two-compartment model mathematical model (5)-(9) was expressed in the dimensionless form by rescaling time, space [25,31,43]. The following governing dimensionless parameters were obtained:

$$\begin{gathered} x^* = \frac{x}{a_1}, \quad t^* = \frac{D_{S_1} t}{a_1^2}, \quad S_0^* = \frac{S_0}{K_M}, \quad K_I^* = \frac{K_I}{K_M}, \\ S_i^* = \frac{S_i}{K_M}, \quad P_i^* = \frac{P_i}{K_M}, \quad i = 1, 2, \\ \sigma^2 = \frac{V_{\max} d_1^2}{K_M D_{S_1}}, \quad \beta_S = \frac{D_{S_2} d_1}{\theta_S D_{S_1} d_2}, \quad \beta_P = \frac{D_{P_2} d_1}{\theta_P D_{P_1} d_2}, \\ I^*(t^*) = \frac{I(t)\, d_1}{n_e F D_{S_1} K_M}, \quad I_{ss}^* = \lim_{t^* \to \infty} I^*(t^*), \end{gathered} \tag{15}$$

where σ^2 is the dimensionless Damköhler number (the Thiele modulus squared) or the diffusion module, β_S and β_P are the Biot numbers for the substrate and product, respectively [34,69,72,73]. The model equations (5)-(9) in dimensionless form are presented in the Appendix. All the dimensional and dimensionless model parameters are listed in Table A1.

The dimensionless factor σ^2 essentially compares the rate of intrinsic enzyme reaction ($V_{\max}/K_M$) with the rate of diffusion through the enzyme layer (D_{S_1}/d_1^2). The enzyme kinetics controls the biosensor response when $\sigma^2 \ll 1$, while the response is under internal diffusion control or limitation when $\sigma^2 \gg 1$ [2,8,34,42,73]. Rearranging the expression of σ^2 gives the timescales of the enzymatic reaction and internal diffusion.

The Biot number is a dimensionless parameter widely used to compare the relative transport resistances of external and internal diffusion [9,41,42,44,45,72]. Since the mass transport properties of the substrate and product are generally different, separate Biot numbers have been introduced, although they are often assumed to be identical [41,43–45,48,74]. The mass transport by diffusion in the enzyme layer is slower than in the diffusion layer at large Biot number values, while low values indicate slower diffusion in the diffusion layer than in the enzyme layer [9,42,72].

2.5. Numerical Simulation

Due to the nonlinearity of the governing equations (5) the initial boundary value problem (5)–(11) can be analytically solved only for specific values of the model parameters [10,34,55]. Hence, the problem was solved numerically.

To find a numerical solution to the problem (5)–(11), a non-uniform discrete grid was introduced in space and time. A semi-implicit linear finite difference scheme has been built as a result of the difference approximation of the model equations [25,31,75]. The resulting system of linear algebraic equations was solved efficiently by the Thomas (the tridiagonal matrix) algorithm [55]. To have an

 doi:10.20944/preprints202505.1693.v1

accurate and stable result, it was required to use a small step size in x direction at the boundaries $x = 0$, $x = a_1$ and $x = a_2$, where the concentration gradients are larger than the gradients away from those boundaries. Further from these boundaries, an exponentially increasing step size was used [25,48,74].

Although the time step is restricted by the partition conditions (8) [76–78], it was reasonable to apply an increasing step size in the time direction [79], as the biosensor action follows the steady-state assumption as $t \to \infty$. The final step size in time was in a few orders of magnitude higher than the first one [43]. The density I_{ss} of the steady-state output current was approximated by the output current calculated at the moment, when the normalized absolute current slope value fell below a given small value 0.001 [25,34].

The numerical simulator has been programmed in Java language [80]. The numerical solution was validated using exact analytical solutions known for specific cases of the first and zero-order reaction rates at the steady-state conditions [34,43] and numerical solutions derived for a two-compartment model of amperometric biosensors at transient conditions [10,31,34]. Approximate analytical solutions, obtained for the corresponding one-compartment model of biosensors with substrate inhibition at steady-state [28,36,37] and transient conditions [33], were also used for validation of the numerical solution.

The simulation results have been visualized using Origin [81].

3. Results and Discusion

To investigate the non-monotonic behavior of amperometric enzyme-based biosensors under uncompetitive substrate inhibition, in conjunction with internal and external diffusion limitations, the biosensor action was simulated across a wide range of key dimensionless model parameter values, using the following typical assumptions for the parameter values: [1,30,31,43,48]:

$$\begin{gathered} D_{P_1} = D_{S_1} = 400\,\mu\text{m}^2/\text{s}, \quad D_{P_2} = D_{S_2} = 600\,\mu\text{m}^2/\text{s}, \\ \theta_P = \theta_S = \theta, \quad \beta_P = \beta_S = \beta, \\ d_1 = 20\,\mu\text{m}, \quad d_2 = 300\,\mu\text{m}, \quad K_M = 100\,\mu\text{M}, \quad n_e = 1. \end{gathered} \tag{16}$$

3.1. Temporal Dynamics of Biosensor Response

Figure 2 shows typical temporal dynamics of the biosensor current I simulated at the following ten values of the substrate concentration S_0: 0.1, 0.2, 0.3, 0.4, 0.5, 0.6, 0.7, 1, 2 and 3 mM, with fixed parameters $V_{\max}$ = 100 µM/s, θ = 0.75, and $K_I = K_M$, in both types of analysis, injection (IA) and batch (BA). The corresponding normalized values $S_0^* = S_0/K_M$ of the substrate concentration are indicated on the curves in Figure 2. All the other model parameters were defined in (16). These simulations were performed under mixed control, involving both enzyme kinetics and internal diffusion ($\sigma^2 = 1$). On the other hand, mass transport in the outer diffusion layer was slower than in the enzyme layer, as indicated by $\beta = 0.13$.

One can see in Figure 2 a noticeable difference in the dynamics of the biosensor response when changing the substrate concentration S_0. The shape of the curves also depends significantly on the mode of analysis, i.e., on the initial conditions (10) or (11). However, the steady-state response is independent of the analysis mode, as the steady-state solution of the initial boundary value problem (5)–(8) is unaffected by those initial conditions [8,25,34,55].

At the beginning of biosensor operation, the output current becomes noticeably slower in IA mode than in BA mode. The delay consists of about 6 - 10 s. This delay in the transient response can be attributed to the diffusion time required for the substrate to pass through the outer diffusion layer and reach the enzyme layer in IA mode [4,29,59]. In contrast, in BA, the substrate contacts the enzyme layer immediately at $t = 0$. The corresponding steady-state times are approximately the same, though they noticeably depend on the substrate concentration.

 doi:10.20944/preprints202505.1693.v1

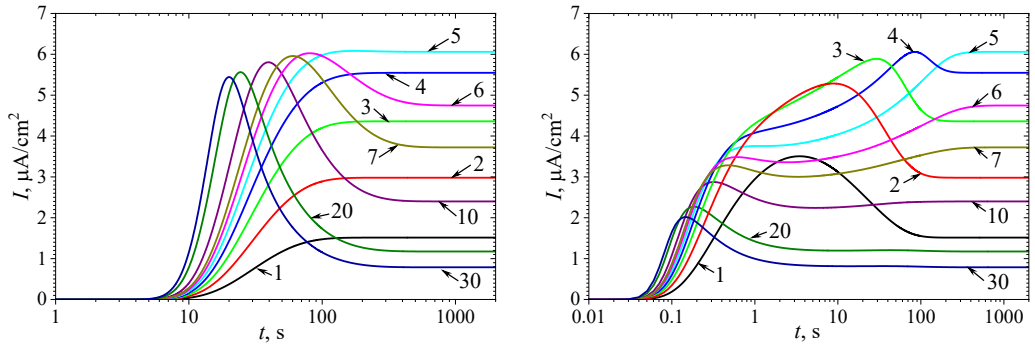

(**a**) (**b**)

Figure 2. Dynamics of the output current $I(t)$ at ten values of the normalized substrate concentration S_0^*, as indicated on the curves, with fixed parameters V_{max} = 100 μM/s, θ = 0.75, and $K_I = K_M$, in IA (**a**) and BA (**b**) modes. Other parameters are defined in (16).

In IA (Figure 2(**a**)), at relatively high substrate concentrations ($S_0^* > 5$), the response follows a three-phase pattern: starting from zero, reaching a maximum, and finally decreasing to a steady value. The output current, after reaching its maximum, enters the descending limb of the bell-shaped curve characteristic of substrate inhibition. In the case of low and moderate substrate concentrations ($S_0^* \leq 5$ in Figure 2(**a**)), the biosensor current monotonically approaches steady-state. On the other hand, Figure 2(**a**) shows nonmonotonic behavior of the steady-state current. At substrate concentrations corresponding to the three-phase pattern ($S_0^* > 5$), the steady-state current decreases with increasing S_0^*, whereas at lower concentrations ($S_0^* \leq 5$), it increases with increasing S_0^*. These aspects of the biosensor with uncompetitive substrate inhibition are well known [19,26,30–33].

Figure 2(**b**) shows noticeably more complex dynamics of the biosensor current in BA mode than in IA. Even at relatively low substrate concentrations ($1 \leq S_0^* \leq 4$), the output current is nonmonotonic. At slightly greater concentration $S_0^* = 5$, the output current becomes a monotonously increasing function of time t, but has an extra inflection point ($t \approx 2$ s) where the curve changes from concave down to concave up.

In the case of relatively high substrate concentrations ($6 \leq S_0^* \leq 10$), the biosensor response exhibits a local minimum and follows a four-phase pattern. At higher concentrations $S_0^* \geq 20$, the response approaches even a five-phase pattern, although the oscillations at $t > 10$ are only slight. Specifically, at $S_0^* = 20$ the transient current $I(t)$ starts from zero, reaches a global maximum of 2.27 μA/cm² at $t = 0.18$ s, decreases to a local minimum of 1.196 μA/cm² at $t = 10.5$ s, increases to a local maximum of 1.206 μA/cm² at $t = 42$ s, and finally decreases to a steady value of 1.17 μA/cm². Thus, the variation between the local extrema and the steady value is only $2 - 3\%$. At a higher concentration of $S_0^* = 30$, this variation is even smaller.

3.2. Effect of Internal Diffusion Limitation

Figure 2 shows the influence of substrate concentration on the dynamics of output current at a fixed maximal enzymatic rate of V_{max} = 100 μM/s, which corresponds to a diffusion module equal to unity ($\sigma^2 = 1$). To investigate the effect of the diffusion module on the transient response of the amperometric biosensors, the response was simulated at very different values of V_{max}. This allowed the transition from enzyme kinetics control ($\sigma^2 \ll 1$) to internal diffusion control ($\sigma^2 \gg 1$) to be observed, while keeping all other parameters the same as those used in the simulations depicted in Figure 2. Figure 3 shows the number N_{ext} of extrema calculated from the simulated responses in both modes of analysis, IA and BA.

 doi:10.20944/preprints202505.1693.v1

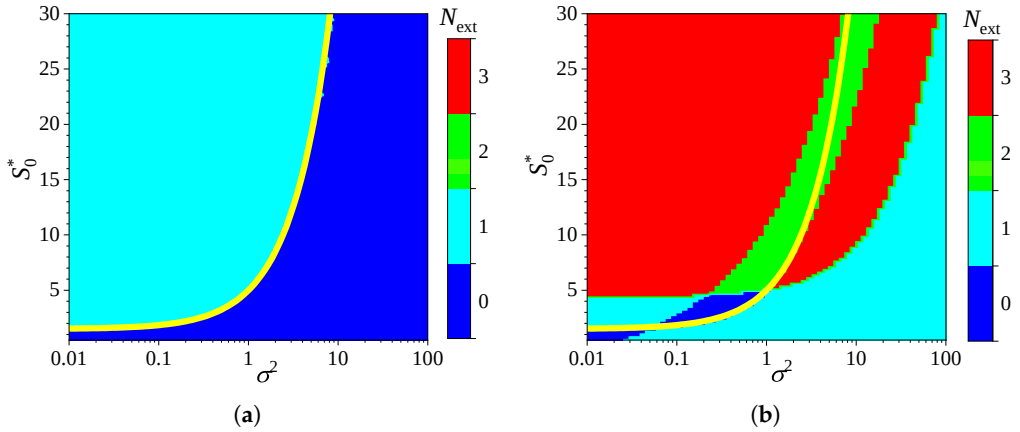

Figure 3. Number N_{ext} of extrema of the output current vs. the diffusion module σ^2 and the normalized substrate concentration S_0^*, with fixed parameters $\theta = 0.75$ and $K_I = K_M$, for IA (**a**) mode and BA (**b**) mode. Other parameters are defined in (16). The yellow line is defined in (17).

As one can see in Figure 3(**a**), the transient output current exhibits one or even no local extremum in IA, when the diffusion module changes in four orders of magnitude, from 0.01 to 100, and the dimensionless substrate concentration S_0^* changes from 1 to 30. When the biosensor acts under the internal diffusion limitation ($\sigma^2 \gg 1$), the response follows a two-phase pattern ($N_{ext} = 0$): starting from zero increases to a steady value. A three-phase pattern ($N_{ext} = 1$) is observed when the biosensor response is governed by enzyme kinetics or mixed control ($\sigma^2 \lesssim 10$), although it also depends on the substrate concentration. The yellow line in Figure 3 represents an approximate boundary between the two values of N_{ext}, 0 and 1, i.e., between model parameter values that result in either two-phase or three-phase patterns. This yellow line is a linear approximation of the boundary,

$$S_0^* = 1.5 + 3.5\sigma^2. \tag{17}$$

The relationship (17) between the substrate concentration and the diffusion module σ^2, resulting in changes in the number of response phases, is approximately linear when the biosensor operates in IA mode, as defined by (17) (Figure 3(**a**)). Similar dependences of the substrate concentration on the diffusion module have already been observed [26,31,33,39,40]. In particular, it was found that the minimum dimensionless substrate concentration at which the response reaches its maximum is a monotonically increasing function of σ^2 [31]. In the case of BA (Figure 3(**b**)), that relation is noticeably more complicated as the number N_{ext} of extrema varies between zero and three, indicating that the number of phases in the response pattern ranges between two and five. In particular, at $\sigma^2 = 1$, increasing the normalized substrate concentration S_0^* from 1 to 30 results in the number N_{ext} of extrema changing in the following sequence: 1, 0, 1, 2, 3. This can also be noticed in Figure 2(**b**).

Although the variation in the number of extrema N_{ext} differs noticeably among the analysis modes, at relatively low substrate concentrations ($S_0^* \lesssim 4.5$) and very low values of the diffusion module ($\sigma^2 \lesssim 0.03$), the number N_{ext} is practically invariant across analysis mode, as observed in the lower left corners of Figures 3(**a**) and 3(**b**).

To observe the effect of the diffusion module σ^2 on the shape of the transient response, the biosensor action was simulated at different values of σ^2, while keeping the substrate concentration fixed at a relatively high level ($S_0^* = 10K_I^* = 10$, $S_0 = 10K_I$), where the inhibition plays a significant role in the biosensor response. The simulation results are shown in Figure 4.

 doi:10.20944/preprints202505.1693.v1

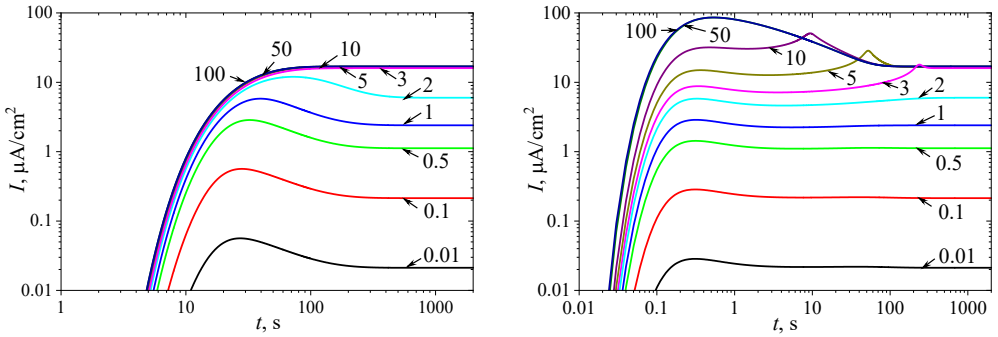

Figure 4. Dynamics of the output current $I(t)$ at ten values of the diffusion module σ^2, as indicated on the curves, with a fixed substrate concentration $S_0^* = 10$, in IA (**a**) mode and BA (**b**) mode. Other parameters are the same as in Figure 3.

One can see in Figure 4(**a**), in IA, the transient output current exhibits a global maximum for $\sigma^2 < 3$, whereas it is a monotonously increasing function of time t for greater values of the diffusion module σ^2, as it was predicted in Figure 3(**a**). In BA (Figure 4(**b**)), for $\sigma^2 < 3$, the shape of $I(t)$ is similar to that observed in IA mode (Figure 4(**a**)), although the function $I(t)$ in BA has additional local extremums, which are close to steady values. However, at slightly greater values of σ^2 ($3 \leq \sigma^2 \leq 10$), the transient current $I(t)$ ehibits a noticeable peak in BA. At high values of the diffusion module ($\sigma^2 > 20$), when the response is govern by internal diffusion control, the output current exhibits only a global maximum, following a two-phase pattern.

On the other hand, at high values of the diffusion module ($\sigma^2 > 5$), the transient response in IA becomes practically invariant to σ^2, whereas in BA, the response dynamics still noticeably depend on σ^2. Maintaining the analytical capability of biosensors for as long as possible is very important [2,4,7]. Typically, the maximal enzymatic rate $V_{\max}$ decreases over time due to enzyme inactivation [70,82]. Therefore, ensuring the stability of the biosensor response (the biosensor resistance) across a range of $V_{\max}$ values is crucial [25,33,37,39,40,82]. Since $V_{\max}$ directly influences σ^2, it is essential to maintain a stable response even when σ^2 undergoes slight variations.

In particular, at two significantly different values of σ^2, namely 0.5 and 5, the response of a biosensor operating under BA conditions follows a five-phase pattern ($N_{\text{ext}} = 3$). However, in the case of $\sigma^2 = 0.5$ (and for $\sigma^2 < 0.5$ as well), the local minimum is barely noticeable, whereas for $\sigma^2 = 5$, all extrema and all five phases are clearly observable. This is particularly important in practical applications of amperometric biosensors, as oscillations in the biosensor response may complicate the use of the calibration curve [15,16]. On the other hand, analyzing both the steady-state and the maximal biosensor currents can significantly extend the calibration curve when using intelligent biosensors [15,30,31,83].

3.3. Effect of External Diffusion Limitation

To investigate the influence of external diffusion limitations on the behavior of amperometric enzyme-based biosensors, the biosensor response was simulated by varying the partition coefficient θ over two orders of magnitude, from 0.01 to 1.0. This variation caused the governing dimensionless Biot number β to change from 0.1 to 10, representing a shift from external to internal mass transfer dominance [9,72]. The substrate concentration S_0 was also independently varied from 0.025 to 3 mM. Simulations were conducted for both types of analysis, injection (IA) and batch (BA), using fixed parameters of $V_{\max} = 100\ \mu\text{M/s}$ and $K_I = K_M$. Figure 5 shows the number N_{ext} of extrema calculated from the simulated responses.

 doi:10.20944/preprints202505.1693.v1

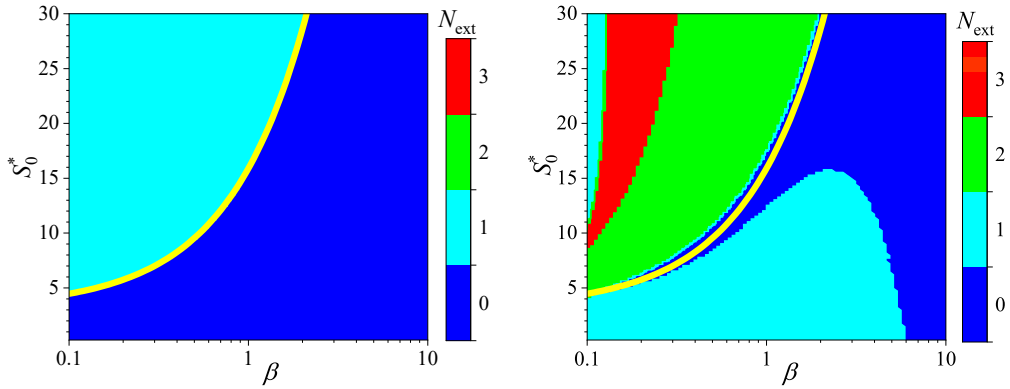

Figure 5. Number N_{ext} of extrema of the biosensor current vs. the Biot number β and the normalized substrate concentration S_0^*, with fixed parameters V_{max} = 100 μM/s, and $K_I = K_M$, for IA (**a**) mode and BA (**b**) mode. Other parameters are defined in (16). The yellow line is defined in (18).

As one can see in Figure 5(**a**), in IA, the dependence of the number N_{ext} of extrema of the transient current on the Biot number is rather similar in shape to that on the diffusion module σ^2. In IA, when the mass transport by diffusion in the diffusion layer is notably faster than in the enzyme layer ($\beta \gtrsim 2$), the response follows a two-phase pattern ($N_{ext} = 0$). At smaller values of β, when the diffusion in the outer diffusion layer is comparable with or slower than that in the enzyme layer ($\beta \lesssim 1$), the response follows a three-phase pattern ($N_{ext} = 1$), although it also depends on the substrate concentration. The yellow line in Figure 5(**a**) represents an approximate boundary between the two values of N_{ext}, 0 and 1,

$$S_0^* = 3.2 + 12.7\beta. \tag{18}$$

In the case of BA (Figure 5(**b**)), the relationship between the number N_{ext} of extrema, the Biot number β, and the substrate concentration is noticeably more complex. The number N_{ext} varies between zero and three, and the boundary between the regions where $N_{ext} = 0$ and $N_{ext} = 1$ is clearly nonlinear. Nevertheless, the boundary (yellow line) between areas indicated as $N_{ext} = 0$ and $N_{ext} = 2$ is similar to that observed in IA (Figure 5(**a**)) between $N_{ext} = 0$ and $N_{ext} = 1$. At relatively high substrate concentrations ($S_0^* \gtrsim 15$), the number of response phases is the same in both modes of analysis, IA and BA, except when $0.15 \lesssim \beta \lesssim 2$, where the number of phases in BA is greater than in IA.

To observe the effect of the Biot number β on the shape of the transient response, the biosensor performance was simulated at nine values of β, while keeping the substrate concentration fixed at a relatively high level ($S_0^* = 10K_I^* = 10$). The simulation results are shown in Figure 6.

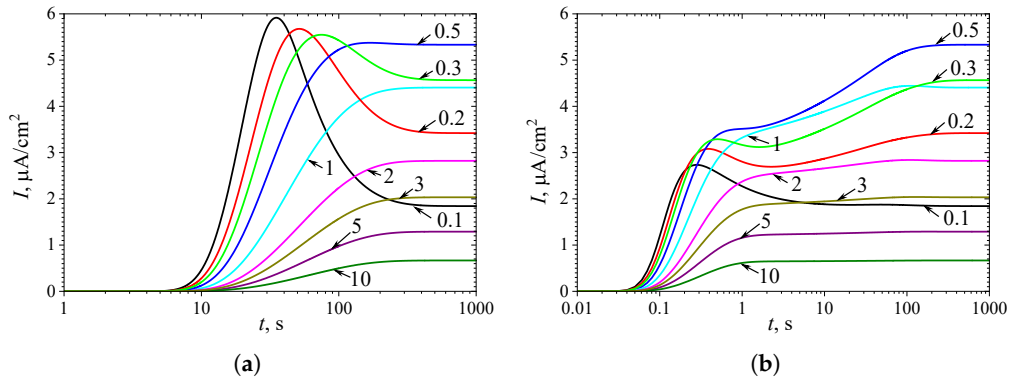

Figure 6. Dynamics of the output current $I(t)$ at nine values of the Biot number β, as indicated on the curves, with with a fixed substrate concentration $S_0^* = 10$, in IA (**a**) mode and BA (**b**) mode. Other parameters are the same as in Figure 5.

 doi:10.20944/preprints202505.1693.v1

Figure 6(**a**) shows, that in IA at $S_0^* = 10$, the transient biosensor current exhibits a global maximum for $\beta \leq 0.5$, whereas it is a monotonously increasing function of time t for greater values of the Biot number β, as it was also shown in Figure 5(**a**).

In BA (Figure 6(**b**)), three extrema can be observed only for the smallest value of the Biot number of $\beta = 0.1$. However, a local minimum and local maximum differ by less than 1 percent. At $\beta = 0.5$ no local extrema are observed but an extra inflection point ($t \approx 2$ s) is observed where the curve changes from concave down to concave up. When $1 \leq \beta \leq 3$, the transient output current has only one global maximum ($N_{\text{ext}} = 1$), which occurs noticeably later (at $t \approx 100$ s) than global maximum observed for small values of β (at $t < 1$ s), and is close to steady-state value. For larger values of β ($\beta > 3$), the global maximum decreasingly approaches the steady-state value.

In addition to the Biot number β, the external Thiele modulus σ_{ext} (also known as the external Damköhler number and the external diffusion module) is used to compare external and internal mass transport resistances. It relates the characteristic timescale of enzymatic reaction within the enzyme layer to that of external mass transfer, i.e., it represents the ratio between the first-order surface reaction rate ($V_{\max}\theta_S / K_M d_1$) and the rate of the mass transfer through the external diffusion layer (D_{S_2}/d_2) [16,30,44,45]. If $\sigma_{\text{ext}}^2 \ll 1$, then the external mass transfer is fast, and the system acts in a reaction-limited regime. The enzymatic reaction is fast, and the external diffusion is limiting when $\sigma_{\text{ext}}^2 \gg 1$. The internal and external Thiele moduli are related through the Biot number for the mass transfer,

$$\sigma_{\text{ext}}^2 = \frac{V_{\max}\theta_S d_1 d_2}{K_M D_{S_2}} = \frac{\sigma^2}{\beta_S}. \tag{19}$$

The effect of the external Thiele modulus on the behavior of amperometric enzyme-based biosensors was not investigated separately, as it is represented through two other dimensionless parameters: the diffusion module σ^2, and the Biot number $\beta = \beta_S$.

3.4. Effect of Inhibition

To investigate the effect of inhibition on the behavior of the biosensor transient current, the biosensor response was simulated by varying the inhibition constant K_I over four orders of magnitude, from 1 µM to 10 mM, thereby changing the normalized inhibition constant K_I^* from 0.01 to 100. The substrate concentration S_0 was independently varied from 0.025 to 3 mM, as in numerical experiments discussed above. Simulations were conducted for both types of analysis, injection (IA) and batch (BA), using fixed parameters of $V_{\max}$ = 100 µM/s and $\theta = 0.75$. At these parameter values, the diffusion module $\sigma^2 = 1$, and the Biot number $\beta = 0.13$. Figure 7 shows the calculated number N_{ext} of extrema.

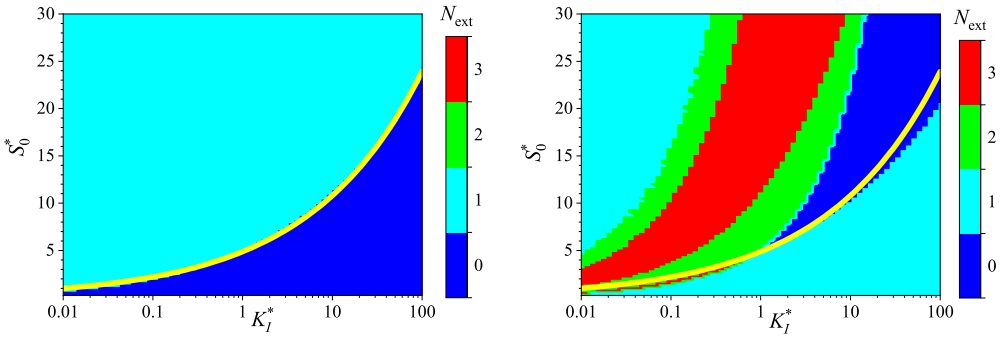

Figure 7. Number N_{ext} of extrema of the biosensor current vs. the normalized inhibition constant K_I^* and the normalized substrate concentration S_0^*, with fixed parameters $V_{\max}$ = 100 µM/s, and $\theta = 0.75$, for IA (**a**) mode and BA (**b**) mode. Other parameters are defined in (16).

 doi:10.20944/preprints202505.1693.v1

As one can see in Figure 7, the dependence of the number N_{ext} of extrema of the transient current on the inhibition constant differs noticeably from those on the diffusion module σ^2 (Figure 3) and the Biot number β (Figure 5).

In IA (Figure 7(a)), the response follows a three-phase pattern ($N_{\text{ext}} = 1$) in most of the entire region of parameter values, $(S_0^*, K_I^*) \in [0.25, 30] \times [0.01, 100]$. Only at relatively low substrate concentrations and large values of the inhibition constant, the response follows a two-phase pattern ($N_{\text{ext}} = 0$), as in the Michaelis-Menten kinetics. This behavior is reasonable because the influence of inhibition decreases with an increasing inhibition constant. Nevertheless, an increase in the inhibition constant can be compensated for by an increase in the substrate concentration. In a particular case of $K_I^* = 10$, the inhibitory term S^2/K_I in the reaction rate equation (4) becomes significant when $S_0^* \geq K_I^*$. The relationship between S_0^* and K_I^* is nonlinear. The yellow line in Figure 7(a) represents an approximate boundary between the two values of N_{ext}, 0 and 1. This line is a power-law (allometric) approximation of the boundary,

$$S_0^* = 4.9 \times K_I^{*0.345}. \tag{20}$$

As shown in Figure 7, in the region parameter values S_0^* and K_I^* where $N_{\text{ext}} = 0$ in IA (i.e., below the yellow line), $N_{\text{ext}} = 1$ in BA.

Figure 7(a) shows that, in the particular case of $K_I^* = 1$, the transient output current in IA is a monotonically increasing function of time for concentrations $S_0^* \lesssim 5$, and become a non-monotonic function (with $N_{\text{ext}} = 1$) at higher concentrations. In the corresponding BA (Figure 7(b)), the number N_{ext} changes with increasing substrate concentration in the following sequence: 1, 0, 2, 3. Notably, $N_{\text{ext}} = 0$ occurs in the specific case of $S_0^* = 5$. The current dynamics in these cases are also illustrated in Figure 2.

To observe the effect of the inhibition constant K_I^* on the dynamics of the transient current, the biosensor action was simulated at eleven different K_I^* values, with the constant substrate concentration held at $S_0^* = 10$. The simulation results are depicted in Figure 8.

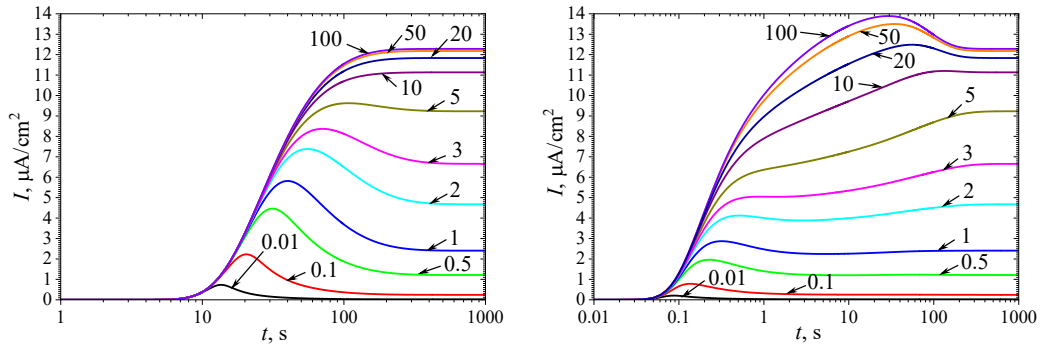

Figure 8. Dynamics of the output current $I(t)$ at eleven values of normalized inhibition constant K_I^*, as indicated on the curves, with with a fixed substrate concentration $S_0^* = 10$, in IA (**a**) mode and BA (**b**) mode. Other parameters are the same as in Figure 7.

As seen in Figures 8(a) and 7(a), in IA at $S_0^* = 10$, the transient current exhibits a global maximum for all values of the inhibition constant K_I^* less than 8. Only when K_I^* becomes comparable to or greater than the concentration S_0^* ($K_I^* \gtrsim S_0^*$) does the output current become a monotonically increasing function of time t.

In BA (Figures 6(b) and 7(b)), the transient current at $S_0^* = 10$ is monotonic only within a relatively narrow range of the inhibition constant K_I^*, approximately between 3 and 8. The number of extrema $N_{\text{ext}} = 3$ is observed when K_I^* varies approximately between 0.1 and 0.9. However, the local minimum and maximum differ from the steady-state by only 1 - 2%, although the global maximum is noticeably

 doi:10.20944/preprints202505.1693.v1

more pronounced. Such small deviations in local extrema from the steady value can be considered perturbations of the response, influencing the response analysis procedure [15,30,31,83].

4. Conclusions

The two-compartment mathematical model (5)–(11) of amperometric enzyme-based biosensors is useful for investigating the influence of uncompetitive substrate inhibition, in conjunction with internal and external diffusion limitations, on the biosensor response. Deriving the corresponding dimensionless form of the model (A1)–(A7) reveals the main governing dimensionless parameters (15).

The dynamics of the enzymatic system shown in Figure 1 are highly sensitive to internal and external diffusion limitations, enzyme inhibition, and, most notably, the mode of analysis. In injection analysis (IA, real-time monitoring), where the arrival of the analyte initiates the biosensor transient response, the response follows a two- or three-phase pattern. In batch analysis (BA), where the biosensor is directly immersed in a buffer solution containing the analyte, the response may exhibit up to five phases. The number N_{ext} of extrema in the transient output current, as defined by equation (14), is useful for determining the conditions under which the biosensor response follows a multi-phase pattern. The steady-state biosensor current is invariant with respect to the analysis mode (Figure 2).

The non-monotonic (three-phase, $N_{\text{ext}} = 1$) transient output current of biosensors operating in IA is observed only when the enzyme kinetics predominate in the biosensor response, compared to the internal diffusion, or when the operation is under mixed control (diffusion module $\sigma^2 \lesssim 10$) (Figure 3(**a**)), the diffusion in the outer diffusion layer is comparable to or slower than that in the enzyme layer (the Biot number $\beta \lesssim 1$) (Figure 5(**a**)), and the substrate concentration is comparable to or greater than the inhibition constant (Figure 7(**a**)), where the current shows a global maximum greater than a steady value (Figures 4(**a**), 6(**a**) and 8(**a**)).

In BA, the monotonic (two-phase, $N_{\text{ext}} = 0$) transient current is observed only when the biosensor response is notably governed by enzyme kinetics ($\sigma^2 < 1$), mass transport by diffusion in the diffusion layer is faster than in the enzyme layer ($\beta \gtrsim 1$), and under specific values of other parameters. Under conditions where biosensors operating in IA follow a three-phase pattern, the transient current in BA can exhibit a maximum five-phase pattern ($N_{\text{ext}} = 3$) (Figures 3(**b**), 5(**b**) and 7(**b**)), where the current shows a global maximum, a local minimum, and a local maximum. The global maximum may occur either before or after a local minimum (Figures 4(**b**), 6(**b**) and 8(**b**)).

Oscillations in the transient biosensor response, caused by substrate inhibition and both internal and external diffusion limitations, should be taken into consideration when using the biosensor calibration curve.

Funding: This research received no external funding.

Institutional Review Board Statement: Not applicable.

Informed Consent Statement: Not applicable.

Data Availability Statement: The study did not report any data.

Acknowledgments: The author sincerely thanks Professors Emeritus Juozas Kulys and Feliksas Ivanauskas for their valuable discussions and contributions to the modeling of biosensors.

Conflicts of Interest: The author declares no conflicts of interest.

 doi:10.20944/preprints202505.1693.v1

Abbreviations

The following abbreviations are used in this manuscript:

E	Enzyme
S	Substrate
P	Reaction product
ES	Enzyme-substrate complex
ESI	Inhibitory complex
IA	Injection analysis
BA	Batch analysis
QSSA	Quasi-steady-state approximation

Appendix A. Dimensionless Mathematical Model

The two-compartment model (5)-(11) was expressed in the dimensionless form by rescaling the time, space, concentrations, and diffusion coefficients as defined in Table A1.

The governing equations (5) in the dimensionless form were then expressed as follows ($t^* > 0$):

$$\begin{aligned} \frac{\partial S_1^*}{\partial t^*} &= \frac{\partial^2 S_1^*}{\partial x^{*2}} - \sigma^2 \frac{S_1^*}{1 + S_1^* + S_1^{*2}/K_I^*}, \\ \frac{\partial P_1^*}{\partial t^*} &= D_{P_1}^* \frac{\partial^2 P_1^*}{\partial x^{*2}} + \sigma^2 \frac{S_1^*}{1 + S_1^* + S_1^{*2}/K_I^*}, \quad x^* \in (0,\, 1), \end{aligned} \tag{A1}$$

where $D_{P_1}^* = D_{P_2}/D_{S_1}$.

The diffusion equations (6) take the following form ($t^* > 0$):

$$\begin{aligned} \frac{\partial S_2^*}{\partial t^*} &= D_{S_2}^* \frac{\partial^2 S_2^*}{\partial x^{*2}}, \\ \frac{\partial P_2^*}{\partial t^*} &= D_{P_2}^* \frac{\partial^2 P_2^*}{\partial x^{*2}}, \quad x^* \in (1,\, a_2^*), \end{aligned} \tag{A2}$$

where $D_{S_2}^* = D_{S_2}/D_{S_1}$, $D_{P_2}^* = D_{P_2}/D_{S_1}$, $a_2^* = a_2/a_1$.

The boundary conditions (7), (8) and (9) are rewritten as follows ($t^* > 0$):

$$S_2^*(a_2^*, t^*) = S_0^*, \quad P_2^*(a_2^*,\, t^*) = 0, \tag{A3}$$

$$\begin{aligned} \left.\frac{\partial S_1^*}{\partial x^*}\right|_{x^*=1} &= D_{S_2}^* \left.\frac{\partial S_2^*}{\partial x^*}\right|_{x^*=1}, \quad S_1^*(1, t^*) = \theta_S S_2^*(1, t^*), \\ \left.\frac{\partial P_1^*}{\partial x^*}\right|_{x^*=1} &= D_{P_2}^* \left.\frac{\partial P_2^*}{\partial x^*}\right|_{x^*=1}, \quad P_1^*(1, t^*) = \theta_P P_2^*(1, t^*), \end{aligned} \tag{A4}$$

$$P_1^*(0, t^*) = 0, \quad \left.\frac{\partial S_1^*}{\partial x^*}\right|_{x^*=0} = 0. \tag{A5}$$

The initial conditions specific to IA, as given in (10), take the following form:

$$\begin{aligned} &S_1^*(x^*, 0) = 0, \quad P_1^*(x^*, 0) = 0, \quad x^* \in [0,\, 1], \\ &S_2^*(x^*, 0) = 0, \quad P_2^*(x^*, 0) = 0, \quad x^* \in [1, a_2^*), \\ &S_2^*(a_2^*,\, 0) = S_0^*, \quad P_2^*(a_2^*,\, 0) = 0. \end{aligned} \tag{A6}$$

The initial conditions (11), which are specific to BA, are transformed to the following conditions:

$$\begin{aligned} &S_1^*(x^*, 0) = 0, \quad P_1^*(x, 0) = 0, \quad x^* \in [0,\, 1), \\ &S_1^*(1,\, 0) = \theta_S S_0^*, \quad P_1^*(1,\, 0) = 0, \\ &S_2^*(x^*, 0) = S_0^*, \quad P_2^*(x^*, 0) = 0, \quad x^* \in [1, a_2^*]. \end{aligned} \tag{A7}$$

 doi:10.20944/preprints202505.1693.v1

Table A1. Dimensional and dimensionless parameters.

Parameter	Dimensional	Dimensionless
Time	t, s	$t^* = D_{S_1} t / a_1^2$
Distance from electrode	x, µm	$x^* = x / a_1$
Enzyme layer thickness	d_1, µm	$d_1^* = d_1 / a_1 = 1$
Diffusion layer thickness	d_2, µm	$d_2^* = d_2 / a_1$
Substrate concentration in enzyme layer	S_1, µM	$S_1^* = S_1 / K_M$
Product concentration in enzyme layer	P_1, µM	$P_1^* = P_1 / K_M$
Substrate concentration in diffusion layer	S_2, µM	$S_2^* = S_2 / K_M$
Product concentration in diffusion layer	P_2, µM	$P_2^* = P_2 / K_M$
Substrate concentration in bulk	S_0, µM	$S_0^* = S_0 / K_M$
Michaelis-Menten constant	K_M, µM	$K_M^* = K_M / K_M = 1$
Substrate inhibition constant	K_I, µM	$K_I^* = K_I / K_M$
Maximal enzymatic rate	$V_{\max}$, µM/s	
Current density	I, µA/cm^2	$I^* = I d_1 / (n_e F D_{S_1} K_M)$
Steady-state current density	I_{ss}, µA/cm^2	$I_{\text{ss}}^* = I_{\text{ss}} d_1 / (n_e F D_{S_1} K_M)$
Diffusion coefficient of substrate in enzyme layer	D_{S_1}, µm^2/s	$D_{S_1}^* = D_{S_1} / D_{S_1} = 1$
Diffusion coefficient of product in enzyme layer	D_{P_1}, µm^2/s	$D_{P_1}^* = D_{P_1} / D_{S_1}$
Diffusion coefficient of substrate in diffusion layer	D_{S_2}, µm^2/s	$D_{S_2}^* = D_{S_2} / D_{S_1}$
Diffusion coefficient of product in diffusion layer	D_{P_2}, µm^2/s	$D_{P_2}^* = D_{P_2} / D_{S_1}$
Partition coefficient for substrate		θ_S
Partition coefficient for product		θ_P
Biot number for substrate		$\beta_S = D_{S_2} d_1 / (\theta_S D_{S_1} d_2)$
Biot number for product		$\beta_P = D_{P_2} d_1 / (\theta_P D_{P_1} d_2)$
Diffusion module		$\sigma^2 = V_{\max} d_1^2 / (K_M D_{S_1})$
External diffusion module		$\sigma_{\text{ext}}^2 = \sigma^2 / \beta_S$

References

1. Bisswanger, H. *Enzyme Kinetics: Principles and Methods*, 2 ed.; Wiley-Blackwell: Weinheim, Germany, 2008.
2. Malhotra, B.D.; Pandey, C.M. *Biosensors: Fundamentals and Applications*; Smithers Rapra: Shawbury, 2017.
3. Patra, S.; Kundu, D.; Gogoi, M., Eds. *Enzyme-based Biosensors: Recent Advances and Applications in Healthcare*; Springer Verlag: Singapore, 2023.
4. Scheller, F.W.; Schubert, F. *Biosensors*; Elsevier Science: Amsterdam, 1992.
5. Sadana, A.; Sadana, N. *Handbook of Biosensors and Biosensor Kinetics*; Elsevier: Amsterdam, The Netherlands, 2011.
6. Cornish-Bowden, A. *Fundamentals of Enzyme Kinetics*, 3 ed.; Portland Press: London, 2004.
7. Turner, A.P.F.; Karube, I.; Wilson, G.S., Eds. *Biosensors: Fundamentals and Applications*; Oxford University Press: Oxford, 1990.
8. Bartlett, P.N. *Bioelectrochemistry: Fundamentals, Experimental Techniques and Applications*; John Wiley & Sons: Chichester, UK, 2008.
9. Banica, F.G. *Chemical Sensors and Biosensors: Fundamentals and Applications*; John Wiley & Sons: Chichester, UK, 2012.
10. Rafat, N.; Satoh, P.; Worden, R.M. Electrochemical Biosensor for Markers of Neurological Esterase Inhibition. *Biosensors-Basel* **2021**, *11*, 459.

 doi:10.20944/preprints202505.1693.v1

11. Gullo, L.; Brunelleschi, B.; Duranti, L.; Fiore, L.; Mazzaracchio, V.; Arduini, F. 3D printed shamrock-like electrochemical biosensing tool based on enzymatic inhibition for on-line nerve agent measurement in drinking water. *Biosens. Bioelectron.* **2025**, *282*, 117471.
12. Dixon, M.; Webb, E.; Thorne, C.; Tipton, K. *Enzymes*, 3 ed.; Longman: London, 1979.
13. Croce, R.A.J.; Vaddiraju, S.; Papadimitrakopoulos, F.; Jain, F.C. Theoretical analysis of the performance of glucose sensors with layer-by-layer assembled outer membranes. *Sensors* **2012**, *12*, 13402–13416.
14. Dagan, O.; Bercovici, M. Simulation tool coupling nonlinear electrophoresis and reaction kinetics for design and optimization of biosensors. *Anal. Chem.* **2014**, *86*, 7835.
15. Baronas, R.; Kulys, J.; Lančinskas, A.; Žilinskas, A. Effect of diffusion limitations on multianalyte determination from biased biosensor response. *Sensors* **2014**, *14*, 4634–4656.
16. Kulys, J. Biosensor response at mixed enzyme kinetics and external diffusion limitation in case of substrate inhibition. *Nonlinear Anal. Model. Control.* **2006**, *11*, 385–392.
17. Mirón, J.; González, M.P.; Vázquez, J.A.; Pastrana, L.; Murado, M.A. A mathematical model for glucose oxidase kinetics, including inhibitory, deactivant and diffusional effects, and their interactions. *Enzyme Microb. Technol.* **2004**, *34*, 513–522.
18. Attaallah, R.; Amine, A. The Kinetic and Analytical Aspects of Enzyme Competitive Inhibition: Sensing of Tyrosinase Inhibitors. *Biosensors-Basel* **2021**, *11*, 322.
19. Forastiere, D.; Falasco, G.; Esposito, M. Strong current response to slow modulation: A metabolic case-study. *J. Chem. Phys.* **2020**, *152*, 134101.
20. Boshagh, F.; Rostami, K.; van Niel, E.W. Application of kinetic models in dark fermentative hydrogen production – A critical review. *Int. J. Hydrog. Energy* **2022**, *47*, 21952–21968.
21. Meraz, M.; Alvarez-Ramirez, J.; Vernon-Carter, E.J.; Reyes, I.; Hernandez-Jaimes, C.; Martinez-Martinez, F. A Two Competing Substrates Michaelis-Menten Kinetics Scheme for the Analysis of In Vitro Starch Digestograms. *Starch-Starke* **2020**, p. 1900170.
22. Meriç, S.; Tünay, O.; San, H.A. A new approach to modelling substrate inhibition. *Environ. Technol.* **2002**, *23*, 163–177.
23. Meriç, S.; Tünay, O.T.; San, H.A. Modelling approaches in substrate inhibition. *Fresenius Environ. Bull.* **1998**, *7*, 183–189.
24. Zhang, S.; Zhao, H.; John, R. Development of a quantitative relationship between inhibition percentage and both incubation time and inhibitor concentration for inhibition biosensors-theoretical and practical considerations. *Biosens. Bioelectron.* **2001**, *16*, 1119–1126.
25. Baronas, R.; Ivanauskas, F.; Kulys, J. *Mathematical Modeling of Biosensors*; Vol. 9, *Springer Series on Chemical Sensors and Biosensors*, Springer: Cham, 2021; p. 456.
26. Achi, F.; Bourouina-Bacha, S.; Bourouina, M.; Amine, A. Mathematical model and numerical simulation of inhibition based biosensor for the detection of Hg(II). *Sens. Actuator B: Chem.* **2015**, *207*, 413–423.
27. Kernevez, J. *Enzyme Mathematics. Studies in Mathematics and its Applications*; Elsevier Science: Amsterdam, 1980.
28. Manimozhi, P.; Subbiah, A.; Rajendran, L. Solution of steady-state substrate concentration in the action of biosensor response at mixed enzyme kinetics. *Sensor. Actuat. B-Chem.* **2010**, *147*.
29. Murray, J.D. *Mathematical Biology: I. An Introduction*, 3 ed.; Springer: New York, 2002.
30. Kulys, J.; Baronas, R. Modelling of amperometric biosensors in the case of substrate inhibition. *Sensors* **2006**, *6*, 1513–1522.
31. Šimelevičius, D.; Baronas, R. Computational modelling of amperometric biosensors in the case of substrate and product inhibition. *J. Math. Chem.* **2010**, *47*, 430–445.
32. Reed, M.C.; Lieb, A.; Nijhout, H.F. The biological significance of substrate inhibition: A mechanism with diverse functions. *BioEssays* **2010**, *32*, 422–429.
33. Mohanasundaraganesan, M.; Luis, J.; Guirao, G.; Rathinama, S. Theoretical Analysis of Amperometric Biosensor with Substrate and Product Inhibition Involving non-Michaelis-Menten Kinetics. *MATCH Commun. Math. Comput. Chem.* **2025**, *93*, 319–347.
34. Schulmeister, T. Mathematical modelling of the dynamic behaviour of amperometric enzyme electrodes. *Sel. Electrode Rev.* **1990**, *12*, 203–260.
35. Romero, M.R.; Baruzzi, A.M.; Garay, F. Mathematical modeling and experimental results of a sandwich-type amperometric biosensor. *Sensors and Actuators B* **2012**, *162*, 284–291.

 doi:10.20944/preprints202505.1693.v1

36. Devi, M.C.; Pirabaharan, P.; Rajendran, L.; Abukhaled, M. Amperometric biosensors in an uncompetitive inhibition processes: a complete theoretical and numerical analysis. *React. Kinet. Mech. Catal.* **2021**, *133*, 655–668.
37. Swaminathan, R.; Devi, M.C.; Rajendran, L.; Venugopal, K. Sensitivity and resistance of amperometric biosensors in substrate inhibition processes. *J. Electroanal. Chem.* **2021**, *895*, 115527.
38. Vinayagan, J.A.; Krishnan, S.M.; Rajendran, L.; Eswari, A. Incorporating different enzyme kinetics in amperometric biosensor for the steady-state conditions: A complete theoretical and numerical approach. *Int. J. Electrochem. Sci.* **2024**, *19*, 100693.
39. Reena, A.; Karpagavalli, S.; Swaminathan, R. Mathematical analysis of urea amperometric biosensor with Non-Competitive inhibition for Non-Linear Reaction-Diffusion equations with Michaelis-Menten kinetics. *Results Chem.* **2024**, *7*, 101320.
40. Mallikarjuna, M.; Senthamarai, R. An amperometric biosensor and its steady state current in the case of substrate and product inhibition: Taylors series method and Adomian decomposition method. *J. Electroanal. Chem.* **2023**, *946*, 117699.
41. Al-Shannag, M.; Al-Qodah, Z.; Herrero, J.; Humphrey, J.A.; Giralt, F. Using a wall-driven flow to reduce the external mass-transfer resistance of a bio-reaction system. *Biochem. Eng. J.* **2008**, *39*, 554–565.
42. Skrzypacz, P.; Kabduali, B.; Golman, B.; Andreev, V. Dead-core solutions and critical Thiele modulus for slabs with a distributed catalyst and external mass transfer. *React. Chem. Eng.* **2023**, *8*, 758–762.
43. Baronas, R. Nonlinear effects of diffusion limitations on the response and sensitivity of amperometric biosensors. *Electrochim. Acta* **2017**, *240*, 399–407.
44. Fang, Y.; Govid, R. New Thiele's Modulus for the Monod Biofilm Model. *Chin. J. Chem. Eng.* **2008**, *16*, 277–286.
45. Gómez-Barea, A.; Leckner, B. Modeling of biomass gasification in fluidized bed. *Prog. Energy Combust. Sci.* **2010**, *36*, 444–509.
46. Hickson, R.I.; Barry, S.I.; Mercer, G.N.; Sidhu, H.S. Finite difference schemes for multilayer diffusion. *Math. Comput. Model.* **2011**, *54*, 210–220.
47. Ašeris, V.; Baronas, R.; Petrauskas, K. Computational modelling of three-layered biosensor based on chemically modified electrode. *Comp. Appl. Math.* **2016**, *35*, 405–421.
48. Baronas, R. Nonlinear effects of partitioning and diffusion-limiting phenomena on the response and sensitivity of three-layer amperometric biosensors. *Electrochim. Acta* **2024**, *478*, 143830.
49. Blaedel, W.J.; Kissel, T.R.; C.Boguslaski, R. Kinetic behavior of enzymes immobilized in artificial membranes. *Anal. Chem.* **1972**, *44*, 2030–2037.
50. Jochum, P.; Kowalski, B.R. A coupled two-compartment model for immobilized enzyme electrodes. *Anal. Chim. Acta* **1982**, *144*, 25–38.
51. Ivanauskas, F.; Baronas, R. Modeling an amperometric biosensor acting in a flowing liquid. *Int. J. Numer. Meth. Fluids* **2008**, *56*, 1313–1319.
52. Do, T.Q.N.; Varnićic, M.; Hanke-Rauschenbach, R.; Vidakovic-Koch, T.; Sundmacher, K. Mathematical modeling of a porous enzymatic electrode with direct electron transfer mechanism. *Electrochim. Acta* **2014**, *137*, 616–629.
53. Rafat, N.; Satoh, P.; Worden, R.M. Integrated Experimental and Theoretical Studies on an Electrochemical Immunosensor. *Biosensors-Basel* **2021**, *10*, 144.
54. Saranya, J.; Rajendran, L.; Wang, L.; Fernandez, C. A new mathematical modelling using Homotopy perturbation method to solve nonlinear equations in enzymatic glucose fuel cells. *Chem. Phys. Let.* **2016**, *662*, 317–326.
55. Britz, D.; Strutwolf, J. *Digital Simulation in Electrochemistry*, 4 ed.; Springer: Berlin, 2016; p. 492.
56. Samarskii, A. *The Theory of Difference Schemes*; Marcel Dekker: New York-Basel, 2001.
57. Gunawardena, J. Time-scale separation: Michaelis and Menten's old idea, still bearing fruit. *FEBS J.* **2014**, *281*, 473–488.
58. Li, B.; Shen, Y.; Li, B. Quasi-steady-state laws in enzyme kinetics. *J. Phys. Chem. A* **2008**, *112*, 2311–2321.
59. Gutfreund, H. *Kinetics for the Life Sciences*; Cambridge University Press: Cambridge, 1995.
60. Lyons, M.E.G. Transport and kinetics at carbon nanotube – redox enzyme composite modified electrode biosensors. *Int. J. Electrochem. Sci.* **2009**, *4*, 77–103.
61. Schulmeister, T. Mathematical treatment of concentration profiles and anodic current of amperometric enzyme electrodes with chemically amplified response. *Anal. Chim. Acta.* **1987**, *201*, 305–310.
62. Wang, J. *Analytical Electrochemistry*, 3 ed.; Wiley: New-York, 2006.

 doi:10.20944/preprints202505.1693.v1

63. Velkovsky, M.; Snider, R.; Cliffel, D.E.; Wikswo, J.P. Modeling the measurements of cellular fluxes in microbioreactor devices using thin enzyme electrodes. *J. Math. Chem.* **2011**, *49*, 251–275.
64. Jobst, G.; Moser, I.; Urban, G. Numerical simulation of multi-layered enzymatic sensors. *Biosens. Bioelectron.* **1996**, *11*, 111–117.
65. Coche-Guerente, L.; Labbé, P.; Mengeaud, V. Amplification of amperometric biosensor responses by electrochemical substrate recycling. 3. Theoretical and experimental study of the phenol-polyphenol oxidase system immobilized in laponite hydrogels and layer-by-layer self-assembled structures. *Anal. Chem.* **2001**, *73*, 3206–3218.
66. Trevelyan, P.M.J.; Strier, D.E.; Wit, A.D. Analytical asymptotic solutions of $nA + mB \rightarrow C$ reaction-diffusion equations in two-layer systems: A general study. *Phys. Rev. E* **2008**, *78*, 026122.
67. Rumsey, T.R.; McCarthy, K.L. Modeling oil migration in two-layer chocolate-almond confectionery products. *J. Food Eng.* **2012**, *111*, 149–155.
68. Lauverjat, C.; de Loubens, C.; Déléris, I.; Tréléa, I.C.; Souchon, I. Rapid determination of partition and diffusion properties for salt and aroma compounds in complex food matrices. *J. Food Eng.* **2009**, *93*, 407–415.
69. Kulys, J. The development of new analytical systems based on biocatalysts. *Anal. Lett.* **1981**, *14*, 377–397.
70. Ruzicka, J.; Hansen, E. *Flow Injection Analysis*; John Wiley & Sons: New York, 1988.
71. Baronas, R.; Ivanauskas, F.; Kulys, J. Modelling dynamics of amperometric biosensors in batch and flow injection analysis. *J. Math. Chem.* **2002**, *32*, 225–237.
72. Lyons, M.E.G.; Bannon, T.; Hinds, G.; Rebouillat, S. Reaction/diffusion with Michaelis-Menten kinetics in electroactive polymer films. Part 2. The transient amperometric response. *Analyst* **1998**, *123*, 1947–1959.
73. Fink, D.; Na, T.; Schultz, J.S. Effectiveness factor calculations for immobilized enzyme catalysts. *Biotechnol. Bioeng.* **1973**, *15*, 879–888.
74. Baronas, R. Nonlinear effects of partitioning and diffusion limitation on the efficiency of three-layer enzyme bioreactors and potentiometric biosensors. *J. Electroanal. Chem.* **2024**, *974*, 118698.
75. Britz, D.; Baronas, R.; Gaidamauskaitė, E.; Ivanauskas, F. Further comparisons of finite difference schemes for computational modelling of biosensors. *Nonlinear Anal. Model. Control* **2009**, *14*, 419–433.
76. Carr, E.J.; March, N.G. Semi-analytical solution of multilayer diffusion problems with time-varying boundary conditions and general interface conditions. *Appl. Math. Comput.* **2018**, *333*, 286–303.
77. March, N.G.; Carr, E.J. Finite volume schemes for multilayer diffusion. *J. Comput. Appl. Math.* **2019**, *345*, 206–223.
78. Lemke, K. Mathematical simulation of an amperometric enzyme-substrate electrode with a pO_2 basic sensor. Part 2. Mathematical simulation of the glucose oxidase glucose electrode. *Med. Biol. Eng. Comput.* **1988**, *26*, 533–540.
79. Bieniasz, L.; Britz, D. Recent developments in digital simulation of electroanalytical experiments. *Pol. J. Chem.* **2004**, *78*, 1195–1219.
80. Moreira, J.E.; Midkiff, S.P.; Gupta, M.; Artigas, P.V.; Snir, M.; Lawrence, R.D. Java programming for high-performance numerical computing. *IBM Syst. J.* **2000**, *39*, 21–56.
81. Moberly, J.; Bernards, M.; Waynant, K. Key features and updates for Origin 2018. *J. Cheminform.* **2018**, *10*, 5.
82. Kulys, J.; Hansen, H. Carbon-paste biosensors array for long-term glucose measurement. *Biosens. Bioelectron.* **1994**, *9*, 491–500.
83. Cui, F.; Yue, Y.; Zhang, Y.; Zhang, Z.; Zhou, H.S. Advancing Biosensors with Machine Learning. *ACS Sens.* **2020**, *5*, 3346–3364.